In vivo exchange of glucose and lactate between photoreceptors and the retinal pigment epithelium

Daniel T. Hass[1], Elizabeth Giering[2], John Y.S. Han[3], Celia M. Bisbach[4], Kriti Pandey[5], Brian M. Robbings[6], Thomas O. Mundinger[2], Nicholas D. Nolan[7], Stephen H. Tsang[7], Neal S. Peachey[8,9,10], Nancy J. Philp[11], James B. Hurley[1]

[1]Department of Biochemistry, University of Washington, Seattle, WA
[2]VA Hospital Puget Sound, Seattle, WA
[3]Department of Ophthalmology, University of Michigan, Ann Arbor, MI
[4]Department of Ophthalmology, University of Wisconsin – Madison, Madison, WI
[5]Department of Neuroscience, University of Texas - Southwestern, Dallas, TX
[6] Department of Laboratory Medicine and Pathology, University of Washington, Seattle WA
[7]Departments of Biomedical Engineering, Ophthalmology Pathology and Cell Biology, Columbia Stem Cell Initiative, Columbia University, New York, NY
[8]Cole Eye Institute, Cleveland Clinic, Cleveland, OH
[9]VA Northeast Ohio Healthcare System, Cleveland, OH
[10]Department of Ophthalmology, Cleveland Clinic Lerner College of Medicine of Case Western Reserve University, Cleveland, OH
[11]Department of Pathology, Thomas Jefferson University, Philadelphia PA

Abstract

Photoreceptors in the retina of a vertebrate's eye are supported by a tissue adjacent to the retina, the retinal pigment epithelium (RPE). The RPE delivers glucose to the outer retina, consumes photoreceptor outer segments discs, and regenerates 11-cis-retinal. Here we address the question of whether photoreceptors also provide metabolic support to the RPE. We use complementary approaches and animal models to show that glucose is the primary fuel for the retina, that photoreceptors are the primary cell type in the retina to consume glucose, and that lactate derived from photoreceptor glucose consumption is transported to and catabolized by the RPE. These data rigorously support and extend the concept of a metabolic ecosystem between photoreceptors and RPE.

Introduction

Degeneration of rod and cone photoreceptors causes blindness in patients with retinitis pigmentosa and age-related macular degeneration. Proteins encoded by >100 distinct genes linked to these diseases have remarkably diverse biochemical activities. We hypothesize that defects in many of these genes create, either directly or indirectly, metabolic stress in photoreceptors. To address the validity of this idea, we are exploring photoreceptor energy metabolism and the metabolic interactions between photoreceptors and their environment.

Photoreceptors in the outer retina receive nutrients from blood that flows through the fenestrated choriocapillaris just inside the sclera of the eye. Between the photoreceptors and this blood supply there is a monolayer of cells called the retinal pigment epithelium (RPE). The basal and apical plasma membranes of the RPE cells are enriched with the glucose transporter GLUT1 (Takata et al., 1992). Glucose is delivered from circulation to the outer retina via these transporters (Swarup et al., 2019).

Isolated retinas break down glucose through aerobic glycolysis and primarily convert the carbon from glucose into lactate (Warburg, 1925). This process, as opposed to oxidation of glucose

carbons to CO_2 in mitochondria, classically occurs in tumor tissue and is referred to as the Warburg effect (Warburg et al., 1927). Of the cells in the retina, photoreceptors express the same isoforms of glycolytic enzymes that are in tumor cells (Lowry et al., 1961; Lindsay et al., 2014; Casson et al., 2016; Rajala et al., 2016; Rueda et al., 2016). Retinas without photoreceptors consume less glucose and produce less lactate than normal retinas (Graymore, 1960; Reading and Sorsby, 1962; Winkler et al., 2004). These data suggest that aerobic glycolysis is performed by photoreceptors.

In a previous report, we described evidence that RPE cells minimize their consumption of glucose so that more glucose can traverse the RPE to reach the retina (Kanow et al., 2017). We also proposed that lactate produced by photoreceptors can suppress consumption of glucose by RPE cells (Kanow et al., 2017). That proposal was based on the results of *ex vivo* analyses of metabolic flux in retinas, RPE-choroid and cultured RPE cells. Here we tested our proposal more rigorously by using multiple unique mouse models, and by infusing ^{13}C-labeled fuels into mice and quantifying ^{13}C-labeled metabolites in their retinas and RPE-choroid tissues. We show that the retina primarily consumes glucose, that photoreceptors are the main consumers of glucose in the retina, and that lactate, both from circulation and from photoreceptors influences energy metabolism in the RPE.

Results

Retina metabolism is fueled primarily by circulating glucose

Rapid consumption of glucose and production of lactate are key metabolic features of isolated retinas (Warburg, 1925; Winkler, 1981; Ames et al., 1992). An isolated mouse retina incubated in culture medium produces nearly two moles of lactate from each mole of glucose that it consumes (Wang et al., 1997; Hass et al., 2023a). Isolated retinas can oxidize fuels other than glucose (Keen and Chlouverakis, 1965; Winkler, 1981; Chertov et al., 2011; Adijanto et al., 2014; Joyal et al., 2016; Kanow et al., 2017), yet the degree to these fuels are normally used *in vivo* is unknown.

We designed an experiment to compare consumption of several types of fuels by retinas within the eyes of awake, freely moving mice (Hui et al., 2017, 2020). Mice were equipped with jugular vein and carotid artery catheters. We infused glucose fully labeled with ^{13}C ("$^{13}C_6$-glucose" or "m+6 glucose") through the jugular veins. For comparison, in separate experiments we infused $^{13}C_3$-lactate, $^{13}C_4$-succinate, $^{13}C_5$-glutamine, or $^{13}C_4$-malate into jugular vein catheters for four hours (glucose) or two hours (each other fuel). Metabolite concentrations and infusion rates are listed in **Table 1**. **Fig. 1A** shows the experiment scheme, and **Fig. 1B** shows how these fuels integrate into energy metabolism. During the infusion we collected plasma from a carotid artery catheter every 30 minutes. Two or four hours after initiating the infusion, we collected final plasma samples, euthanized each mouse, dissected tissue samples, and froze them in liquid N_2. Isotopic labeling of metabolites in plasma and tissue samples was quantified either by gas chromatography/mass spectrometry (GC-MS) or liquid chromatography/mass spectrometry (LC-MS/MS).

Plasma samples were used to confirm that each infused fuel reached isotopic steady state in circulation (**Supplementary Fig. 1A-E**). At isotopic steady state, we determined the extent to which each infused fuel is used to make m+3 pyruvate (**Fig. 1C**), m+2 citrate (**Fig. 1D**), m+2 glutamate (**Fig. 1E**), and m+2 aspartate (**Fig. 1F**) in the neural retina. The y-axis for these figure panels shows normalized labeling, which is calculated as the fractional enrichment of a metabolite (including all isotopologues) with ^{13}C in the tissue relative to the fractional enrichment of the source of ^{13}C in plasma (Hui et al., 2017, 2020). When the infused fuel is $^{13}C_6$-glucose, a

normalized labeling value for pyruvate of 1.0 would mean that 100% of pyruvate produced in the tissue was produced from glucose that had been taken up from circulating blood.

Metabolic intermediates in the retina are primarily derived from $^{13}C_6$-glucose and $^{13}C_3$-lactate, and poorly labeled from all other sources. m+6 glucose generates circulating m+3 lactate (**Supplementary Fig. 2A**), and carbons from circulating m+3 lactate can contribute to ^{13}C-labeled pyruvate, citrate, glutamate, and malate in the retina (**Fig. 1C-F**). Therefore, a portion of glucose-derived labeling can occur via lactate (Hui et al., 2017). Similarly, ^{13}C-lactate can undergo gluconeogenesis and generate circulating ^{13}C-labeled glucose (**Supplementary Fig. 2B**) (TeSlaa et al., 2021). We calculated the direct contributions of glucose or lactate to the TCA cycle (approximated by averaging ^{13}C labeling on citrate, α-ketoglutarate, glutamate, and aspartate) in the retina using a previously described formula (Described in Supplementary note 3 of (Hui et al., 2017)). This type of analysis produces an unrealistic result, that 114% of the retina's TCA cycle is directly fueled by glucose, and 8.5% by lactate. However, this calculation is impacted by m+1 labeling on TCA cycle intermediates, which is abundant (pink bars in **Supplementary Fig. 2C**). M+1 labeling may be an artifact of $^{13}CO_2$ that was generated by other tissues but recycled in the retina (Duan et al., 2022). When m+1 isotopologues are not included, the revised calculation indicates that glucose and lactate fuel 73.9% and 3.3% of the retina's TCA cycle (**Supplementary Fig. 2D**). The primary message of these calculations is that glucose is the major TCA cycle fuel in the retina, and that the direct contribution of circulating lactate to retina metabolism is small.

Photoreceptors are the main consumers of glucose in the retina.

Previous studies showed that glucose consumption increases while rod photoreceptors are developing within the retina, and decreases when photoreceptors degenerate (Cohen and Noell, 1960; Reading and Sorsby, 1962). We compared rates of glucose consumption by normal retinas (C57BL/6J) vs. by retinas without photoreceptors (*Aipl1*$^{-/-}$ in the C57BL/6J background). *Aipl1*$^{-/-}$ mice are models of Leber congenital amaurosis. In these mice, rod and cone photoreceptors degenerate fully by one month of age (Ramamurthy et al., 2004). We used this model to confirm the contribution of photoreceptors to retina glucose consumption.

We used an enzymatic assay to quantify depletion of glucose from the medium bathing freshly isolated retinas. *Aipl1*$^{-/-}$ retinas deplete glucose from the medium at only 15% of the rate of C57BL/6J controls and they release lactate at 22% of the control rate (**Fig. 2A-B**). We also measured accumulation of $^{13}C_3$ lactate within the isolated retinas when they were incubated in $^{13}C_6$-glucose. The initial rate of ^{13}C lactate accumulation within *Aipl1*$^{-/-}$ retinas is only 11% of the rate of C57BL/6J controls (**Fig. 2C**).

GLUT1 is the only glucose transporter that normally is expressed in detectable amounts in rods (Daniele et al., 2022). If photoreceptors consume most of the glucose provided to retinas, then deletion of Glut1 from photoreceptors should diminish glucose consumption substantially. We determined initial rates of glucose depletion and lactate accumulation in culture medium by retinas from mice in which *Glut1* was conditionally deleted either from the whole retina (Ret∆*Glut1*) or from rods only (Rod∆*Glut1*). Loss of *Glut1* from the entire retina slows the rate of glucose depletion to 30% of the rate of Glut1$^{fl/fl}$ control retinas (**Fig. 2D**) and lactate export to 22% (**Fig. 2E**). In the experiment comparing Rod∆*Glut1* mice to controls, glucose consumption and lactate production were assessed in the presence of 10 mM lactate and 100 μM palmitate-BSA in the KRB buffer bathing retinas. Loss of *Glut1* from rod photoreceptors slows glucose depletion to 26% of *Glut1*$^{fl/fl}$ controls **Fig. 2D**) and lactate export to 53% (**Fig. 2E**). These data confirm that photoreceptors are the primary cell type that takes up glucose and exports lactate, and that they import glucose mostly through GLUT1.

Photoreceptors can use lactate for fuel when glucose is unavailable.
Remarkably, despite being the main consumers of glucose in the retina, rod photoreceptors do not die immediately upon loss of components essential for glycolysis or for uptake of glucose (Chinchore et al., 2017; Daniele et al., 2022; Weh et al., 2023). That suggests that rods can use other fuels when glucose is not available. We hypothesized that under normal conditions oxidation of glucose by a rod consumes NAD^+, so its capacity to import and oxidize lactate is limited. But when glucose is not available for oxidation the cytosolic NAD^+/NADH ratio in rod should increase. A greater abundance of cytosolic NAD^+ could promote oxidation of cytosolic lactate to pyruvate. This would deplete intracellular lactate and generate a gradient of lactate that favors import of extracellular lactate (**Fig 3A**).

We compared fuel preferences of isolated mouse retinas in KRB supplemented with 5 mM glucose, 10 mM lactate, and 100 μM palmitate-BSA. We included palmitate because previous reports had shown that it can be a respiratory fuel for retinas (Joyal et al., 2016). We used three treatment conditions. The overall concentration of each metabolic fuel remained the same across treatment conditions, but in each treatment condition only one of the fuels was labeled with ^{13}C. We isolated retinas from control and Rod∆Glut1 mice and then incubated them for 2 hours in these media. We harvested the retinas, extracted metabolites from them, and used GC-MS to quantify how the carbons from each type of fuel had integrated into metabolic intermediates. ^{13}C from each fuel can integrate its carbons into TCA cycle intermediates, but glucose and lactate substantially outperformed palmitate under these conditions (**Fig. 3B**).

We compared consumption of fuels by control and Rod∆Glut1 retinas. We tested the idea that rods oxidize other fuels when access to glucose is decreased. The absence of GLUT1 in rods substantially influences the abundance of metabolic intermediates in the retina (**Supplementary Fig. 3**), and how well these intermediates were ^{13}C labeled from each fuel (**Fig. 3C-E**). Fractional labeling from ^{13}C glucose decreased for most metabolic intermediates, suggesting a diminished ability of glucose to fuel a portion of retina metabolism (**Fig. 3C**). However, fractional labeling of the glycolytic intermediates 3-PG and PEP increased substantially in the absence of GLUT1 in rods. Notably, it has been reported that Müller cells express low levels of pyruvate kinase (PK) (Lindsay et al., 2014). Abnormally high uptake of ^{13}C glucose into Müller cells could cause a buildup of ^{13}C labeled 3PG and PEP upstream of the PK reaction. A similar finding for *Glut1*-deficient macrophages has been reported (Freemerman et al., 2019).

The absence of GLUT1 in rods limits incorporation of ^{13}C from glucose, but incorporation of ^{13}C from lactate increases (**Fig. 3D**). That finding suggests that lactate consumption increases to compensate for the diminished ability to import glucose into rods. Pyruvate and several other intermediates were labeled more in Rod∆*Glut1* retinas by $^{13}C_3$-lactate. Incorporation of carbons from $^{13}C_{16}$-palmitate decreased in Rod∆*Glut1* retinas, suggesting that glucose and palmitate metabolism in retinas are synergistic (**Fig. 3E**). Our findings suggest that when the supply of glucose to photoreceptors is cut off, photoreceptors instead catabolize lactate.

***In vivo* evidence that RPE imports lactate that has been exported from photoreceptors.**
Normally, photoreceptors are the primary exporters of lactate in mouse retinas. **Figs. 2B** and **2C** show that when fueled with glucose, *Aipl1*$^{-/-}$ retinas export much less lactate than normal retinas. Several groups have demonstrated that RPE can transport lactate, and that lactate RPE transport is essential for retinal health (la Cour et al., 1994; Daniele et al., 2008). Kanow et al. proposed that lactate that has been exported from the retina is metabolized within the RPE (Kanow et al., 2017). That hypothesis was based on findings from *ex vivo* analyses of tissues and cultured RPE cells. We designed an *in vivo* experiment that uses retinas without

205 photoreceptors to test this hypothesis in the eyes of living mice. We predicted that without
206 photoreceptors to export lactate, less lactate will be imported into the RPE-choroid.
207
208 We dissected RPE-choroid tissue from control mice and from two different lines of mice in which
209 photoreceptors had degenerated, *Aipl1*$^{-/-}$ and *Pde6b*$^{H620Q/H620Q}$. *Pde6b*$^{H620Q/H620Q}$ mice are models
210 of retinitis pigmentosa, with a slower form of retinal degeneration than *Aipl1*$^{-/-}$ mice (Davis et al.,
211 2008a). We used GC-MS to quantify the abundance of metabolites in RPE-choroid tissue of
212 these models (**Fig. 4A-F**). Lactate is the only glycolytic metabolite in the RPE-choroid that
213 consistently was less abundant when photoreceptors in the retina had degenerated (**Fig. 4A,D**).
214 This finding further supports the idea that normally the RPE imports lactate made by and
215 released from photoreceptors (Daniele et al., 2008).
216
217 We also tested this idea by quantifying metabolites in RPE-choroid from mice in which GLUT1
218 either is absent from the entire retina (RetΔ*Glut1*), or absent only from rods (RodΔ*Glut1*). As
219 with the models of photoreceptor degeneration, there is less lactate in the RPE-choroid from
220 eyes of these mice (**Fig. 4G-L**). Lactate was not the only metabolite with altered levels in these
221 models, but it was the only metabolite that was altered consistently in the RPE-choroid of all
222 four model systems. In three of four models, there also was an increase in aspartate,
223 suggesting either an increase in retina-derived aspartate, an increase in local aspartate
224 production, or a decrease in local aspartate consumption. We also noted a substantial increase
225 in α-ketoglutarate and glutamine uniquely in the PDE6-deficient RPE-choroid tissue.
226
227 ***In vivo* flux measurements confirm that lactate produced by photoreceptors serves as an**
228 **energetic fuel for RPE-choroid.**
229 The next set of experiments show that AIPL1-deficiency directly affects metabolic flux from
230 glucose only in retina tissue and not in RPE tissue.
231
232 *Ex vivo analysis*: *Aipl1* normally is expressed in photoreceptors and not in RPE cells (van der
233 Spuy et al., 2002). There are no photoreceptors in adult *Aipl1*$^{-/-}$ mouse retinas because they all
234 have degenerated. We isolated retina and RPE-choroid tissue from C57BL/6J and *Aipl1*$^{-/-}$ mice,
235 incubated them separately in 5 mM $^{13}C_6$-glucose and harvested tissues between 0 and 5
236 minutes after beginning the incubation. **Fig. 5A** shows that AIPL1$^{-/-}$ retinas produce much less
237 lactate than control C57BL/6J retinas. **Fig. 5B** shows that lactate production is not altered in
238 RPE-choroid tissue isolated from *Aipl1* $^{-/-}$ mice. Normally, retinal tissue produces much more
239 lactate than RPE-choroid tissue. The slower production of lactate that does occur in the RPE-
240 choroid is not affected by loss of *Aipl1* .
241
242 Those results confirm that photoreceptors must be present for glycolysis to be the dominant
243 metabolic pathway in the retina. AIPL1$^{-/-}$ retinas do not make enough lactate to export it in
244 abundance to the RPE.
245
246 *In vivo analysis:* We hypothesized that lactate imported from photoreceptors normally is a
247 significant fraction of the total lactate in RPE-choroid tissue. Disrupted delivery of glucose-
248 derived lactate from the retina to the RPE would limit the amount of lactate in RPE-choroid. We
249 designed an experiment to test this.
250
251 We infused a bolus dose of 100 mg/kg $^{13}C_6$-glucose into jugular vein catheters in C57BL/6J and
252 *Aipl1* $^{-/-}$ mice. We euthanized mice 1, 2, 3, or 5 minutes following the infusion, and dissected the
253 retina and RPE-choroid. We extracted metabolites from each tissue and used mass
254 spectrometry to quantify the extent to which carbons from $^{13}C_6$-glucose were used to make

glycolytic and mitochondrial intermediates (**Fig. 5C and D**). The result confirms our prediction that much less m+3 lactate reaches the RPE-choroid **(Fig. 5D)** in AIPL1$^{-/-}$ mice than in controls.

Nevertheless, other findings from that *in vivo* experiment were unexpected and puzzling. We found that ^{13}C labeled glycolytic intermediates (DHAP and PEP) upstream of the reaction catalyzed by PK seemed to accumulate both in retinas and in RPE-choroid from AIPL1$^{-/-}$ eyes. That result appeared inconsistent with our *ex vivo* analyses (**Fig. 5A,B**) and our predictions.

Further analyses revealed the explanation for this unexpected observation. There is an unavoidable delay of ~2 minutes between euthanasia and the time when retina and RPE-choroid tissues are fully dissected and frozen. During that interval there is no fresh blood available to the tissues to maintain a supply of glucose. We hypothesized that due to the rapid consumption of glucose by photoreceptors in normal retinas, postmortem metabolism could deplete glycolytic intermediates rapidly in the tissue. Metabolites would be depleted faster in wild-type retinas that have photoreceptors than in AIPL1$^{-/-}$ retinas during the time between euthanasia and tissue harvest.

We performed an *ex vivo* experiment to test this hypothesis. We incubated isolated retinas from C57BL/6J and AIPL1$^{-/-}$ mice for 10 minutes in KRB medium supplemented with 5 mM $^{13}C_6$-glucose. Then we moved the retinas to KRB medium without glucose. We collected retinas at 0, 1, 3, and 5 minutes after moving the tissue, and then quantified glycolytic intermediates. Remarkably, the absolute quantities of ^{13}C-labeled DHAP, 3PG and PEP (black lines in **Supplementary Fig. 4A**) in normal retinas decreased rapidly, 50-70% within the first minute. In contrast, these intermediates were stable in AIPL1$^{-/-}$ retinas (red lines in **Supplementary Fig. 4A)**. We also monitored the fractional labeling of the metabolites (**Supplementary Fig. 4B**)**.** The fractional labeling of early glycolytic intermediates also decreased within the first minute. However, the fractional labeling of later intermediates, pyruvate and lactate remained closer to their initial values at the time that glucose was withdrawn.

This result of this *ex vivo* experiment is consistent with our hypothesis. What had appeared to be accumulation of DHAP and PEP in AIPL1$^{-/-}$ tissues relative to control tissues (**Fig. 5C)** is caused by an artifact. The artifact occurs during the unavoidable delay between euthanasia and harvesting of the tissue. It is caused by very rapid consumption of glucose by photoreceptors in control retinas. That rapid consumption does not occur in AIPL1$^{-/-}$ retinas. The same effect occurs in RPE-choroid tissue after blood flow to the eye has stopped. During that time the wild-type retina, which is in close contact with the RPE, can consume glucose rapidly from the RPE until we separate the tissues in the final step of the dissection.

The *ex vivo* simulation shows that fractional labeling of DHAP and PEP at the time of euthanasia are not well preserved during 1-2 minutes of ischemia (**Supplementary Fig. 4B**). However, fractional labeling of pyruvate and lactate are better preserved. **Fig. 5E** and **F** show the results of the same bolus infusion experiment as in **Fig. 5C and D** but instead of the data being expressed as absolute amounts they are expressed as fractional labeling. It shows that pyruvate and lactate are substantially less labeled both in the retina and in the RPE of mice that lack photoreceptors in their retinas. Even though glycolytic intermediates are depleted faster the RPE-choroid from control mice still have as much as 9 times more lactate **(Fig. 5D)** than the RPE-choroid from eyes that do not have photoreceptors.

In summary, the *in vivo* bolus infusion confirms that less lactate reaches the RPE-choroid when there are no photoreceptors in the retina.

Discussion

Normal vision is dependent on the circulation of carbon between the retina and RPE (Daniele et al., 2008, 2022). The retina and the RPE provide metabolic support for each other (Lakkaraju et al., 2020). Energy from light isomerizes 11-cis retinal to all-trans in the retina (Wald, 1968). The visual cycle in the RPE then uses metabolic energy to regenerate 11-cis retinal for the retina (Saari, 2016). Photoreceptors also use substantial carbon to generate outer segments disks, which constantly turn over and which require glucose transport (Young, 1967; Swarup et al., 2019; Daniele et al., 2022). The RPE also recycles material from the tips of rod outer segments, and it transports ions, nutrients and water to and from the retina (Young and Bok, 1969; Quinn and Miller, 1992; la Cour et al., 1994). In this report we focused on energy metabolism.

In a previous report, we described distinct metabolic features of the retina and RPE and proposed that they are complementary and optimized to ensure that sufficient glucose can traverse the RPE to fuel the retina (Kanow et al., 2017). That hypothesis was based primarily on biochemical measurements from isolated mouse retina tissue, mouse RPE-choroid tissue and cultured human RPE cells. After proposing the hypothesis, which we referred to as a “metabolic ecosystem”, we felt that a more direct demonstration of metabolic relationships in the eye of a living animal would better support this hypothesis. This report describes those tests and several new observations.

We extended our previous findings to show that:

- Retina metabolism in the eye of a living mouse is fueled primarily by circulating glucose and lactate
- Photoreceptors are the main consumers of glucose in the retina
- Photoreceptors can use lactate for fuel when glucose is unavailable
- RPE tissue in the eye of a living mouse imports lactate that has been exported from photoreceptors
- Lactate produced by photoreceptors in the eye of a living mouse can be oxidized to TCA cycle intermediates by RPE-choroid tissue

Why do photoreceptors consume so much glucose?

Photoreceptors hydrolyze ATP to maintain an essential ion gradient across their plasma membrane, and they use the energy extracted from glycolysis to synthesize new ATP (Ames et al., 1992; Okawa et al., 2008; Ingram et al., 2020). We show that most of the glycolytic activity in the retina within the eye of a living mouse happens in photoreceptors. Because photoreceptor and RPE mitochondria consume so much O_2, the steady state concentration of O_2 in the outer retina is very low (Linsenmeier, 1986; Yu and Cringle, 2006). In any biological system, mitochondrial activity is limited by O_2 availability, and glycolysis necessarily becomes a predominant metabolic pathway from which to extract energy from fuels (Gstraunthaler et al., 1999; Gilglioni et al., 2018; Hass et al., 2023b; Tan et al., 2024).

It is possible that retinas benefit from limited availability of O_2. Along with light, O_2 is a major source of retina lipid peroxidation (Wiegand et al., 1983). Maintaining low O_2 levels in the retina could slow or prevent lipid peroxidation. A highly active mitochondrial metabolism in photoreceptors and RPE could therefore help to shield retina lipids from peroxidation.

Glucose also is used in anabolic pathways, and it is necessary for outer segment synthesis (Daniele et al., 2022). It is likely that a far greater proportion of glucose turnover feeds into catabolic pathways than into anabolic pathways. Yet the absence of glucose catabolism does

not result in immediate photoreceptor death (Chinchore et al., 2017; Daniele et al., 2022; Weh et al., 2023), and to an extent, lactate can substitute for glucose as an energetic fuel. This may imply that if there is a defect that impacts glycolysis, increasing lactate supply or catabolism could be a therapeutic mechanism to sustain photoreceptors.

What sustains the RPE? We showed in this report that in the eye of a living animal lactate exported from the retina can be imported into RPE and oxidized in mitochondria. Lactate slows the consumption of glucose in RPE cells and mouse RPE-choroid (Kanow et al., 2017). Lactate may therefore protect glucose from being consumed by the RPE, and allow for more glucose to fuel photoreceptor metabolic activity (Kanow et al., 2017). However, lactate is not the only fuel that RPE cells consume. They metabolize proline (Zhu et al., 2023), succinate (Bisbach et al., 2020; Hass et al., 2022), glutamate (Xu et al., 2020), and fatty acids (Adijanto et al., 2014; Reyes-Reveles et al., 2017). RPE cells also have the ability to store and mobilize glycogen (Senanayake et al., 2006). It will be important to establish the relative contributions of each of these fuels to RPE metabolism in the eye of a living animal and to determine how they are influenced by illumination, circadian factors, aging and disease.

Acknowledgements:

We thank Craig Beight for maintaining the colony of Rod∆Glut1 mice and for injecting tamoxifen.

Funding Support:

DTH is supported by a Brightfocus Foundation Postdoctoral Fellowship (M2022003F) and NEI K99EY034881. JYSH is supported by a Brightfocus Foundation Postdoctoral Fellowship (M2024001F). CMB was supported by F31EY031165. NDN is supported by F31EY033660. SHT is supported by U01EY030580, U01EY034590 R24EY028758, R24EY027285, 5P30EY019007, R01EY033770, R01EY018213, R01EY024698, Piyada Phanaphat fund, Lynette & Richard Jaffe, NYEE Foundation, Foundation Fighting Blindness TA-GT-0321-0802-COLU-TRAP and RPB unrestricted grant. SHT is on the scientific and clinical advisory board for Emendo, Medical Excellence Capital, and Nanoscope Therapeutics. NSP is supported by P30EY015585 and IK6BX005233. NJP is supported by R01EY026525. JBH is supported by NEI R01EY06641, R01EY017863, R21032597 and Foundation Fighting Blindness TA-NMT-0522-0826-UWA-TRAP. This work was supported in part by NIH NIDDK grant P30 DK017047 to the University of Washington Diabetes Research Center and used the Diabetes Research Center - Metabolic and Cellular Phenotyping Core.

Materials and Methods

Ethical approval

This study was carried out in accordance with the National Research Council's Guide for the Care and Use of Laboratory Animals (*8th ed*). For experiments using C57BL6J and AIPL1$^{-/-}$ mice, all protocols were approved by the Institutional Animal Care and Use Committees (IACUC) at the University of Washington and the ACORP at the Veterans Affairs – Puget Sound Health Care System. For experiments using tamoxifen-treated RodΔGlut1 mice and *Glut1*$^{LoxP/LoxP}$ controls, protocols were approved by the IACUC at the Cole Eye Institute of the Cleveland Clinic. For experiments using RetΔGlut1 mice and Glut1$^{LoxP/LoxP}$ controls, protocols were approved by the IACUC at the Thomas Jefferson University. For experiments using Pde6b$^{H620Q/H620Q}$ mice, protocols were approved by the IACUC at Columbia University.

Animals

All experiments adhered to our approved IACUC protocol and the ARVO statement for the use of animals in ophthalmology research. Mice were group housed at an ambient temperature of 25°C, with a 12-hour light cycle, and *ad libitum* access to water and normal rodent chow. We used male and female wild-type C57BL/6J (RRID: IMSR_JAX:000664) mice, and AIPL1$^{-/-}$ mice bred to a C57BL/6J background over a series of at least six back-crosses. Mouse ages ranged from 2-6 months old except for RetΔGlut1, which were used at 1 month of age to avoid significant retinal degeneration. RodΔGlut1 mice were used at 2.5 months of age. We determined *ex vivo* glucose uptake, *ex vivo* lactate release, and metabolite content in tissue from Glut1$^{LoxP/LoxP}$; crx-cre (RetΔGlut1) and *Glut1*$^{LoxP/LoxP}$;*Pde6g-*^{creERT2} (RodΔGlut1) mice. The generation of these transgenic mouse models is described in previous publications (Koch et al., 2015; Daniele et al., 2022). To induce cre recombinase activity in RodΔGlut1 mice, animals were given daily intraperitoneal injections of 100 µg tamoxifen / g body weight over 3 days. Injection formulations were made by dissolving tamoxifen at 100 mg/ml in ethanol and diluting this solution 1:10 in corn oil. Injections were given beginning at 5 weeks of age and were also administered to littermate controls (Glut1$^{LoxP/LoxP}$). *Pde6b*$^{H620Q/H620Q}$ mice were generated as previously described (Davis et al., 2008b) and kept as homozygous breeders.

Euthanasia and tissue dissection

Mice were euthanized by awake cervical dislocation. The time of day for euthanasia was after 11 am, to avoid variability due to peak outer segment phagocytosis. We dissected eyes from the mouse into room temperature Hank's buffered salt solution (Gibco, Cat#: 14170120). Eyes were cleared of extraocular muscle and collagenous tissue and the cornea was separated from the sclera by cutting along the ora serrata. We removed the cornea, iris, and lens, then teased apart the remaining retina and RPE-choroid tissue. This process typically takes ~2-4 minutes for both eyes from one mouse. Retina and RPE-choroid tissue were immediately flash frozen in liquid N_2 (*in vivo* experiments) or used in downstream experiments then flash frozen in liquid N_2 (*ex vivo* metabolic flux).

Installation of jugular vein and carotid artery catheters

The procedure for chronic jugular vein and carotid artery catheterization was performed as previously described (Ayala et al., 2011) by the Metabolic and Cellular Phenotyping Core of the University of Washington's Diabetes Research Center. Briefly, following induction and maintenance under systemic inhaled anesthesia (isoflurane 1.5-2% in 1 mL/min), mice were administered with 4 mg/kg ketoprofen to reduce post-surgical swelling and provide analgesia. For intravenous infusions, jugular veins were isolated through a lateral incision to the trachea, and a silastic catheter was introduced into the vein, anchored to surrounding tissue, tunneled

444 subcutaneously to the nape of the neck and connected to a vascular access port. A subset of
445 mice received a contralateral carotid artery cannulation for blood sampling. The catheters were
446 filled with heparinized saline, the skin incisions were sutured, and the mice recovered for 1 week
447 before conscious infusion studies.
448
449 *Infusions*
450 We infused labeled fuels one of two ways. In the first way (**Fig. 1**, **Supplemental Fig. 1**) jugular
451 catheters were infused gradually through syringes connected to syringe pumps. Metabolites
452 were dissolved in sterile saline and infused at the concentrations and rates listed in table 1.
453
454 **Table 1. Stock concentrations and infusion rates for ^{13}C-labeled fuels.**

Metabolite	Concentration (mM)	Infusion rate (µL/g/min)	Infusion period (min)	Supplier	Catalog #
13C6-glucose	200	0.1	240	Cambridge Isotope Laboratories	CLM-504
13C3-lactate	400	0.1	120		CLM-1579
13C4-succinate	10	0.05	120		CLM-1571
13C5-glutamine	100	0.1	120		CLM-1822-H
13C4-malate	10	0.05	120		CLM-8065-PK

455
456 In addition to long term infusions we administered 100 mg/kg $^{13}C_6$-glucose as a bolus through
457 jugular catheters, over a period of approximately 20 seconds. One, two, three, and five minutes
458 after the start of the infusion, mice were euthanized. Retina and RPE-choroid tissue were
459 dissected and snap frozen in liquid N_2.
460
461 *Ex vivo metabolic flux*
462 Unless otherwise specified, mouse retina and RPE-choroid tissue was incubated in Krebs-
463 Ringer bicarbonate (KRB) buffer (98.5 mM NaCl, 4.9 mM KCl, 1.2 mM KH_2PO_4 1.2 mM $MgSO_4$-
464 $7H_2O$, 20 mM HEPES, 2.6 mM $CaCl_2$-$2H_2O$, 25.9 mM $NaHCO_3$, pH 7.4) supplemented with 5
465 mM U-^{13}C-glucose. This buffer was equilibrated at 37°C, 21% O_2, and 5% CO_2 prior to
466 incubations. We incubated freshly dissected tissue in media at 37°C, 21% O_2, and 5% CO_2 for
467 amounts of time indicated in each figure. Following each incubation, tissue samples were flash
468 frozen in liquid N_2. Medium was sampled every 30 minutes to evaluate glucose and lactate
469 content.
470
471 *Glucose and lactate assays*
472 Glucose and lactate levels in cell culture supernatant were determined enzymatically, as in
473 (Seidemann, 1973) but adapted for use in a 96 well plate. A detailed description of the adapted
474 glucose assay protocol can be found at https://www.protocols.io/view/glucose-concentration-
475 assay-hexokinase-g6pdh-metho-dm6gpj5jdgzp/v1. A detailed description of the adapted lactate
476 assay can be found at https://www.protocols.io/view/lactate-concentration-assay-ldh-method-
477 6qpvr4733gmk/v1. For each assay, levels of glucose or lactate are determined by measuring
478 absorbance of light at 340 nm, which reflects NADH or NADPH produced in the assay. We
479 measured absorption of 340 nm light using a Synergy 4 plate reader (BioTek).
480
481 *Metabolite extraction*
482 Metabolites were separated from tissue in an extraction buffer consisting of 80% methanol, 20%
483 H_2O, and 10 µM methylsuccinate (Sigma, Cat#: M81209) as an internal standard. The
484 extraction buffer was equilibrated on dry ice, and 150 µL was added to each sample. Tissues
485 were then disrupted by sonication and incubated on dry ice for 45 minutes to precipitate protein.
486 Proteins were pelleted at 17,000 × g for 30 minutes at 4°C. The supernatant containing

487 metabolites was lyophilized at room temperature until dry and stored at −80°C until
488 derivatization. The pellet containing protein was resuspended by sonication in RIPA buffer (150
489 mM NaCl, 1.0% Triton X-100, 0.5% sodium deoxycholate, 0.1% SDS, 50 mM Tris, pH 8.0) and
490 protein was determined by a BCA assay (Thermo Fisher, Cat#: 23225).
491
492 *Metabolite derivatization for Gas Chromatography-Mass Spectrometry*
493 Dried samples were derivatized with 10 µL of 20 mg/mL methoxyamine HCl (Sigma, Cat#:
494 226904) dissolved in pyridine (Sigma, Cat#: 270970) and incubated at 37°C for 90 minutes.
495 Samples were further derivatized with 10 µL tert-butyldimethylsilyl-N-methyltrifluoroacetamide
496 (Sigma, Cat#: 394882) and incubating at 70°C for 60 minutes.
497
498 *Gas chromatography-mass spectrometry*
499 Metabolites were analyzed on an Agilent 7890/5975C GC-MS using methods described
500 extensively in previous work (Chertov et al., 2011; Du et al., 2015). One microliter of derivatized
501 sample is injected and delivered to an Agilent HP-5MS column by helium gas (flow rate: 1
502 mL/min). The column temperature starts at 100°C for 4 minutes then increases by 5°C/min to
503 300°C, where it is held for 5 min. We collect ion intensities after a 6.5-min solvent delay.
504 Selected ion monitoring (SIM) records only selected m/z in expected retention time windows.
505 These masses range from m/z: ~50–600. Peaks were integrated in MSD ChemStation (Agilent
506 Technologies, version E.02.01.1177), and correction for natural isotope abundance was
507 performed using IsoCor 1.0 (Millard et al., 2012; Heinrich et al., 2018). Corrected metabolite
508 signals were converted to molar amounts by comparing metabolite peak abundances in
509 samples with those in a 'standard mix' containing known quantities of metabolites. Multiple
510 concentrations of this mix were extracted, derivatized, and run alongside samples in each
511 experiment. These known metabolite concentrations were used to generate a standard curve
512 that allowed for metabolite quantification. Paired tissues such as retinas and RPE-choroid from
513 the same mouse were treated as technical replicates and averaged.
514
515 *Liquid chromatography-mass spectrometry*
516 For liquid chromatography, samples were separated on an Acquity 2D UPLC equipped with an
517 Acuity BEH Amide column (Waters, 2.1 × 50 mm, 1.7 µm). The mobile phases were (A) water
518 with 10 m*M* ammonium acetate (pH 8.9) and (B) acetonitrile/water (95%/5%) with
519 10 m*M* ammonium acetate (pH 8.9). All solvents were LC–MS Optima grade (Fisher
520 Scientific). The protocol was 0 min: [5% A, 95% B], 2 min [15% A, 85% B], 2.8 min: [40% A,
521 60% B], 3.2 min: [50% A, 50% B], 3.7 min: [15% A, 85% B], 4.4 min: [5% A, 95% B], at a flow
522 rate of 0.4 mL/min. Chromatographically separated glucose was quantified on a Waters Xevo
523 TQ mass spectrometer with electrospray ionization. Glucose ions were collected in negative
524 mode with a cone = 18 V, collision energy = 8 V, parent ions of m/z = 179-185 and daughter
525 ions of m/z=89-92. Dwell time for each ion was 0.08 s.
526
527 *Statistical Analysis*
528 All displayed data include mean ± standard error and may additionally show individual
529 experimental replicates. Statistical analyses were performed using Prism (GraphPad Software,
530 version 10.0). Significance thresholds were set to $\alpha<0.05$. When p-values are not directly
531 shown, * indicates $p<0.05$, ** indicates $p<0.01$, *** indicates $p<0.001$. "n" signifies sample size,
532 which is indicated in figure legends for corresponding experiments. For glucose depletion and
533 lactate production in medium (**Fig. 2**), a linear regression was used to calculate slopes for
534 glucose consumption or lactate production over the first hour of the experiment. Slopes were
535 compared using a student's t-test. T-tests were also used to analyze the data in **Fig. 4A-L**.
536 Other data were analyzed by a two-way ANOVA (**Fig 3. C-E**, **Supplemental Fig. 3**). Post-hoc

537 comparisons for 2-way ANOVAs and multiple T-tests (**Fig. 4**) were made using the two-stage
538 step-up method of Benjamini, Krieger, and Yekutieli.
539
540
541 **References**

542 Adijanto J, Du J, Moffat C, Seifert EL, Hurle JB, Philp NJ (2014) The retinal pigment epithelium
543 utilizes fatty acids for ketogenesis. J Biol Chem 289:20570–20582.

544 Ames A, Li YY, Heher EC, Kimble CR (1992) Energy metabolism of rabbit retina as related to
545 function: high cost of Na+ transport. J Neurosci 12:840–853.

546 Ayala JE, Bracy DP, Malabanan C, James FD, Ansari T, Fueger PT, McGuinness OP,
547 Wasserman DH (2011) Hyperinsulinemic-euglycemic clamps in conscious, unrestrained
548 mice. J Vis Exp Available at: https://www.ncbi.nlm.nih.gov/pubmed/22126863.

549 Bisbach CM, Hass DT, Robbings BM, Rountree AM, Sadilek M, Sweet IR, Hurley JB (2020)
550 Succinate Can Shuttle Reducing Power from the Hypoxic Retina to the O2 Rich Pigment
551 Epithelium. Cell Rep 31:107606.

552 Casson RJ, Wood JPM, Han G, Kittipassorn T, Peet DJ, Chidlow G (2016) M-Type Pyruvate
553 Kinase Isoforms and Lactate Dehydrogenase A in the Mammalian Retina: Metabolic
554 Implications. Invest Ophthalmol Vis Sci 57:66–80.

555 Chertov AO, Holzhausen L, Kuok IT, Couron D, Parker E, Linton JD, Sadilek M, Sweet IR,
556 Hurley JB (2011) Roles of glucose in photoreceptor survival. J Biol Chem 286:34700–
557 34711.

558 Chinchore Y, Begaj T, Wu D, Drokhlyansky E, Cepko CL (2017) Glycolytic reliance promotes
559 anabolism in photoreceptors. Elife 6 Available at:
560 https://www.ncbi.nlm.nih.gov/pubmed/28598329.

561 Cohen LH, Noell WK (1960) Glucose catabolism of rabbit retina before and after development
562 of visual function. J Neurochem 5:253–276.

563 Daniele LL, Han JYS, Samuels IS, Komirisetty R, Mehta N, McCord JL, Yu M, Wang Y,
564 Boesze-Battaglia K, Bell BA, Du J, Peachey NS, Philp NJ (2022) Glucose uptake by
565 GLUT1 in photoreceptors is essential for outer segment renewal and rod photoreceptor
566 survival. FASEB J 36:e22428.

567 Daniele LL, Sauer B, Gallagher SM, Pugh EN, Philp NJ (2008) Altered visual function in
568 monocarboxylate transporter 3 (Slc16a8) knockout mice. Am J Physiol Cell Physiol
569 295:C451–C457.

570 Davis RJ, Tosi J, Janisch KM, Kasanuki JM, Wang N-K, Kong J, Tsui I, Cilluffo M, Woodruff
571 ML, Fain GL, Lin C-S, Tsang SH (2008a) Functional Rescue of Degenerating
572 Photoreceptors in Mice Homozygous for a Hypomorphic cGMP Phosphodiesterase 6 b
573 Allele (Pde6bH620Q). Invest Ophthalmol Vis Sci 49:5067–5076.

574 Davis RJ, Tosi J, Janisch KM, Kasanuki JM, Wang N-K, Kong J, Tsui I, Cilluffo M, Woodruff
575 ML, Fain GL, Lin C-S, Tsang SH (2008b) Functional Rescue of Degenerating
576 Photoreceptors in Mice Homozygous for a Hypomorphic cGMP Phosphodiesterase 6 b
577 Allele (Pde6b H620Q). Investigative Ophthalmology & Visual Science 49:5067–5076.

578 Du J, Linton JD, Hurley JB (2015) Probing Metabolism in the Intact Retina Using Stable Isotope
579 Tracers. Methods Enzymol 561:149–170.

580 Duan L, Cooper DE, Scheidemantle G, Locasale JW, Kirsch DG, Liu X (2022) 13C tracer
581 analysis suggests extensive recycling of endogenous CO2 in vivo. Cancer Metab 10:11.

582 Freemerman AJ et al. (2019) Myeloid Slc2a1-Deficient Murine Model Revealed Macrophage
583 Activation and Metabolic Phenotype Are Fueled by GLUT1. The Journal of Immunology
584 202:1265–1286.

585 Gilglioni EH, Chang J, Duijst S, Go S, Adam AAA, Hoekstra R, Verhoeven AJ, Ishii-Iwamoto
586 EL, Oude Elferink RPJ (2018) Improved oxygenation dramatically alters metabolism and
587 gene expression in cultured primary mouse hepatocytes. Hepatol Commun 2:299–312.

588 Graymore C (1960) Metabolism of the developing retina. III. Respiration in the developing
589 normal rat retina and the effect of an inherited degeneration of the retinal
590 neuroepithelium. Br J Ophthalmol 44:363–369.

591 Gstraunthaler G, Seppi T, Pfaller W (1999) Impact of Culture Conditions, Culture Media
592 Volumes, and Glucose Content on Metabolic Properties of Renal Epithelial Cell
593 Cultures : Are Renal Cells in Tissue Culture Hypoxic? Cellular Physiology and
594 Biochemistry 9:150–172.

595 Hass DT, Bisbach CM, Robbings BM, Sadilek M, Sweet IR, Hurley JB (2022) Succinate
596 metabolism in the retinal pigment epithelium uncouples respiration from ATP synthesis.
597 Cell Rep 39:110917.

598 Hass DT, Bisbach CM, Sadilek M, Sweet IR, Hurley JB (2023a) Aerobic Glycolysis in
599 Photoreceptors Supports Energy Demand in the Absence of Mitochondrial Coupling. In:
600 Retinal Degenerative Diseases XIX, 19th ed. (Ash J, Pierce E, Anderson R, Bowes
601 Rickman C, Hollyfield JG, Grimm C, eds). Springer Nature.

602 Hass DT, Zhang Q, Autterson GA, Bryan RA, Hurley JB, Miller JML (2023b) Medium Depth
603 Influences O2 Availability and Metabolism in Human RPE Cultures. Invest Ophthalmol
604 Vis Sci 64:4.

605 Heinrich P, Kohler C, Ellmann L, Kuerner P, Spang R, Oefner PJ, Dettmer K (2018) Correcting
606 for natural isotope abundance and tracer impurity in MS-, MS/MS- and high-resolution-
607 multiple-tracer-data from stable isotope labeling experiments with IsoCorrectoR. Sci Rep
608 8:17910.

609 Hui S, Cowan AJ, Zeng X, Yang L, TeSlaa T, Li X, Bartman C, Zhang Z, Jang C, Wang L, Lu
610 W, Rojas J, Baur J, Rabinowitz JD (2020) Quantitative Fluxomics of Circulating
611 Metabolites. Cell Metab 32:676-688.e4.

612 Hui S, Ghergurovich JM, Morscher RJ, Jang C, Teng X, Lu W, Esparza LA, Reya T, Zhan L,
613 Yanxiang Guo J, White E, Rabinowitz JD (2017) Glucose feeds the TCA cycle via
614 circulating lactate. Nature 551:115–118.

615 Ingram NT, Fain GL, Sampath AP (2020) Elevated energy requirement of cone photoreceptors.
616 Proceedings of the National Academy of Sciences 117:19599–19603.

617 Joyal J-S et al. (2016) Retinal lipid and glucose metabolism dictates angiogenesis through the
618 lipid sensor Ffar1. Nat Med 22:439–445.

619 Kanow MA, Giarmarco MM, Jankowski CS, Tsantilas K, Engel AL, Du J, Linton JD,
620 Farnsworth CC, Sloat SR, Rountree A, Sweet IR, Lindsay KJ, Parker ED, Brockerhoff
621 SE, Sadilek M, Chao JR, Hurley JB (2017) Biochemical adaptations of the retina and
622 retinal pigment epithelium support a metabolic ecosystem in the vertebrate eye. Elife 6
623 Available at: https://www.ncbi.nlm.nih.gov/pubmed/28901286.

624 Keen H, Chlouverakis C (1965) Metabolism of isolated rat retina. The role of non-esterified fatty
625 acid. Biochem J 94:488–493.

626 Koch SF, Tsai Y-T, Duong JK, Wu W-H, Hsu C-W, Wu W-P, Bonet-Ponce L, Lin C-S, Tsang
627 SH (2015) Halting progressive neurodegeneration in advanced retinitis pigmentosa. J
628 Clin Invest 125:3704–3713.

629 la Cour M, Lin H, Kenyon E, Miller SS (1994) Lactate transport in freshly isolated human fetal
630 retinal pigment epithelium. Investigative Ophthalmology & Visual Science 35:434–442.

631 Lakkaraju A, Umapathy A, Tan LX, Daniele L, Philp NJ, Boesze-Battaglia K, Williams DS
632 (2020) The cell biology of the retinal pigment epithelium. Prog Retin Eye Res:100846.

633 Lindsay KJ, Du J, Sloat SR, Contreras L, Linton JD, Turner SJ, Sadilek M, Satrústegui J, Hurley
634 JB (2014) Pyruvate kinase and aspartate-glutamate carrier distributions reveal key
635 metabolic links between neurons and glia in retina. Proc Natl Acad Sci U S A
636 111:15579–15584.

637 Linsenmeier RA (1986) Effects of light and darkness on oxygen distribution and consumption in
638 the cat retina. J Gen Physiol 88:521–542.

639 Lowry OH, Roberts NR, Schulz DW, Clow JE, Clark JR (1961) Quantitative Histochemistry of
640 Retina: II. ENZYMES OF GLUCOSE METABOLISM. Journal of Biological Chemistry
641 236:2813–2820.

642 Millard P, Letisse F, Sokol S, Portais JC (2012) IsoCor: correcting MS data in isotope labeling
643 experiments. Bioinformatics 28:1294–1296.

644 Okawa H, Sampath AP, Laughlin SB, Fain GL (2008) ATP consumption by mammalian rod
645 photoreceptors in darkness and in light. Curr Biol 18:1917–1921.

646 Quinn RH, Miller SS (1992) Ion transport mechanisms in native human retinal pigment
647 epithelium. Invest Ophthalmol Vis Sci 33:3513–3527.

648 Rajala RVS, Rajala A, Kooker C, Wang Y, Anderson RE (2016) The Warburg Effect Mediator
649 Pyruvate Kinase M2 Expression and Regulation in the Retina. Sci Rep 6:37727.

650 Ramamurthy V, Niemi GA, Reh TA, Hurley JB (2004) Leber congenital amaurosis linked to
651 AIPL1: A mouse model reveals destabilization of cGMP phosphodiesterase. Proc Natl
652 Acad Sci U S A 101:13897–13902.

653 Reading HW, Sorsby A (1962) The metabolism of the dystrophic retina—I: Comparative studies
654 on the glucose metabolism of the developing rat retina, normal and dystrophic. Vision
655 Research 2:315–325.

656 Reyes-Reveles J, Dhingra A, Alexander D, Bragin A, Philp NJ, Boesze-Battaglia K (2017)
657 Phagocytosis-dependent ketogenesis in retinal pigment epithelium. J Biol Chem
658 292:8038–8047.

659 Rueda EM, Johnson JE, Giddabasappa A, Swaroop A, Brooks MJ, Sigel I, Chaney SY, Fox DA
660 (2016) The cellular and compartmental profile of mouse retinal glycolysis, tricarboxylic
661 acid cycle, oxidative phosphorylation, and ~P transferring kinases. Mol Vis 22:847–885.

662 Saari JC (2016) Vitamin A and Vision. Subcell Biochem 81:231–259.

663 Seidemann J (1973) Lowry, O. H., und J. V. Passonneau: A flexible system of enzymatic
664 analysis. Academic Press, New York, 1972. 291 S., 32 Abb., 15 Tab., Preis $ 14.00.
665 Starch - Stärke 25:322–322.

666 Senanayake P, Calabro A, Hu JG, Bonilha VL, Darr A, Bok D, Hollyfield JG (2006) Glucose
667 utilization by the retinal pigment epithelium: evidence for rapid uptake and storage in
668 glycogen, followed by glycogen utilization. Exp Eye Res 83:235–246.

669 Swarup A, Samuels IS, Bell BA, Han JYS, Du J, Massenzio E, Abel ED, Boesze-Battaglia K,
670 Peachey NS, Philp NJ (2019) Modulating GLUT1 expression in retinal pigment
671 epithelium decreases glucose levels in the retina: impact on photoreceptors and Müller
672 glial cells. Am J Physiol Cell Physiol 316:C121–C133.

673 Takata K, Kasahara T, Kasahara M, Ezaki O, Hirano H (1992) Ultracytochemical localization of
674 the erythrocyte/HepG2-type glucose transporter (GLUT1) in cells of the blood-retinal
675 barrier in the rat. Investigative Ophthalmology & Visual Science 33:377–383.

676 Tan J et al. (2024) Limited oxygen in standard cell culture alters metabolism and function of
677 differentiated cells. EMBO J 43:2127–2165.

678 TeSlaa T, Bartman CR, Jankowski CSR, Zhang Z, Xu X, Xing X, Wang L, Lu W, Hui S,
679 Rabinowitz JD (2021) The Source of Glycolytic Intermediates in Mammalian Tissues.
680 Cell Metab 33:367-378.e5.

681 van der Spuy J, Chapple JP, Clark BJ, Luthert PJ, Sethi CS, Cheetham ME (2002) The Leber
682 congenital amaurosis gene product AIPL1 is localized exclusively in rod photoreceptors
683 of the adult human retina. Hum Mol Genet 11:823–831.

684 Wald G (1968) The Molecular Basis of Visual Excitation. Nature 219:800–807.

685 Wang L, Kondo M, Bill A (1997) Glucose metabolism in cat outer retina. Effects of light and
686 hyperoxia. Investigative Ophthalmology & Visual Science 38:48–55.

687 Warburg O (1925) The Metabolism of Carcinoma Cells. Cancer Research 9:16.

688 Warburg O, Wind F, Negelein E (1927) THE METABOLISM OF TUMORS IN THE BODY. J
689 Gen Physiol 8:519–530.

690 Weh E, Goswami M, Chaudhury S, Fernando R, Miller N, Hager H, Sheskey S, Sharma V,
691 Wubben TJ, Besirli CG (2023) Metabolic Alterations Caused by Simultaneous Loss of
692 HK2 and PKM2 Leads to Photoreceptor Dysfunction and Degeneration. Cells 12:2043.

693 Wiegand RD, Giusto NM, Rapp LM, Anderson RE (1983) Evidence for rod outer segment lipid
694 peroxidation following constant illumination of the rat retina. Investigative
695 Ophthalmology & Visual Science 24:1433–1435.

696 Winkler BS (1981) Glycolytic and oxidative metabolism in relation to retinal function. J Gen
697 Physiol 77:667–692.

698 Winkler BS, Sauer MW, Starnes CA (2004) Effects of L-glutamate/D-aspartate and monensin on
699 lactic acid production in retina and cultured retinal Müller cells. J Neurochem 89:514–
700 525.

701 Xu R, Ritz BK, Wang Y, Huang J, Zhao C, Gong K, Liu X, Du J (2020) The retina and retinal
702 pigment epithelium differ in nitrogen metabolism and are metabolically connected.
703 Journal of Biological Chemistry 295:2324–2335.

704 Young RW (1967) The renewal of photoreceptor cell outer segments. J Cell Biol 33:61–72.

705 Young RW, Bok D (1969) Participation of the retinal pigment epithelium in the rod outer
706 segment renewal process. J Cell Biol 42:392–403.

707 Yu DY, Cringle SJ (2006) Oxygen distribution in the mouse retina. Invest Ophthalmol Vis Sci
708 47:1109–1112.

709 Zhu S, Xu R, Engel AL, Wang Y, McNeel R, Hurley JB, Chao JR, Du J (2023) Proline provides
710 a nitrogen source in the retinal pigment epithelium to synthesize and export amino acids

711 for the neural retina. bioRxiv Available at:
712 https://www.ncbi.nlm.nih.gov/pubmed/37131780.

713
714 **Figure Legends**
715
716 **Figure 1. Glucose is the primary fuel for retina metabolism.** Jugular vein and carotid artery
717 catheters were installed in C57BL/6J mice. After mice had recovered from the surgery, they
718 were infused with $^{13}C_6$-glucose, $^{13}C_3$-lactate, $^{13}C_5$-glutamine, $^{13}C_4$-succinate, and $^{13}C_4$-malate.
719 Infusion parameters are listed in **Table 1**. Shown in the figure are schematics of (**A**) the setup
720 for infusion experiments, and (**B**) the pathways through which infused fuels (highlighted by
721 yellow ovals) integrate into energy metabolism. Each circle represents a carbon atom on an
722 intermediate in these pathways. Blue circles represent labeling patterns from glucose or lactate,
723 while purple circles represent labeling patterns from glutamine, succinate, and malate. After
724 mice are infused with each tracer, they are euthanized and their retinas dissected then. Tissue
725 and plasma samples are analyzed by mass spectrometry. **C-F** show the labeling of (**C**)
726 pyruvate, (**D**) citrate, (**E**) glutamate, and (**F**) aspartate from infused $^{13}C_6$-glucose (n=4), $^{13}C_3$-
727 lactate (n=7), $^{13}C_5$-glutamine (n=4), $^{13}C_4$-succinate (n=4) or $^{13}C_4$-malate (n=4). "Normalized
728 labeling" indicates the labeling of the metabolic intermediate in the figure panel divided by the
729 labeling of the infused intermediate in circulation. This normalization method accounts for
730 differences in the proportion of circulating fuel in the bloodstream.
731
732 **Figure 2. Photoreceptors are the main consumers of glucose in the retina.** Retinas were
733 dissected from eyes then incubated in Krebs-Ringer Bicarbonate buffer supplemented with 5
734 mM glucose, at 37°C and 5% CO_2. Glucose consumption from medium (**A**, **D**, **F**) and lactate
735 production (**B**, **E**, **G**) were monitored over 1-1.5 hours. These assays were used to determine
736 how glycolytic metabolism is affected by (**A**, **B**) photoreceptor degeneration due to loss of AIPL1
737 (n=3-4), (**D**, **E**) loss of Glut1 from the retina (n=4-5), or (**F**, **G**) loss of Glut1 from rod
738 photoreceptors (n=5). Loss of photoreceptors, loss of retinal Glut1, or loss of rod Glut1 slowed
739 retina glucose utilization. (**C**) C57BL/6J and AIPL1$^{-/-}$ retinas were also incubated in KRB
740 supplemented with 5 mM $^{13}C_6$-glucose. Retina tissue was flash-frozen 0, 0.5, 1, 3, or 5 minutes
741 after the start of the incubation. Labeling of metabolic intermediates in the retina was assessed
742 by mass spectrometry. Labeling of lactate with ^{13}C from glucose is slowed by the loss of
743 photoreceptors (n=3-4 retinas / time point).
744
745 **Figure 3. When retinas cannot consume glucose, they consume more lactate.** Mice lacking
746 Glut1 in rod photoreceptors (RodΔGlut1) and identically treated littermate control mice were
747 euthanized, and retinas dissected. Retinas were incubated for 2 hours in KRB supplemented
748 with 5 mM glucose, 10 mM lactate, or 100 μM palmitate-BSA. In this experiment, source of ^{13}C
749 was $^{13}C_6$-glucose for one cohort of retinas, $^{13}C_3$-lactate for the second cohort, or $^{13}C_{16}$-palmitate
750 in a third cohort. Following the incubation, retinas were flash-frozen in liquid N_2 and later
751 analyzed by mass spectrometry. Our hypothesis is that loss of glucose metabolism in rods
752 would increase metabolism from the other fuel sources by altering NAD^+/NADH. This hypothesis
753 is illustrated in (**A**). (**B**) in control retinas, the level of labeling on PEP, alanine, pyruvate, citrate,
754 glutamine, malate, or aspartate from $^{13}C_6$-glucose, $^{13}C_3$-lactate, or $^{13}C_{16}$-palmitate. Glucose and
755 lactate are the most prevalent sources of ^{13}C. Fractional labeling of glycolytic, TCA cycle
756 intermediates, and amino acids in control and RodΔGlut1 retinas from (**C**) $^{13}C_6$-glucose (n=3-4),
757 (**D**) $^{13}C_3$-lactate (n=3-4), or (**E**) $^{13}C_{16}$-palmitate (n=4). Data are displayed as a fold-change from
758 labeling in control retinas.
759

760 **Figure 4. When photoreceptors do not consume glucose, there is a decrease in RPE-**
761 **choroid lactate.** *Aipl1*$^{-/-}$, *Pde6b*^{H620Q}, RetΔGlut1, RodΔGlut1, and control mice were
762 euthanized and RPE-choroid tissue was immediately dissected from the eye and flash-frozen.
763 Tissue metabolite levels were analyzed using mass spectrometry, and divided into three
764 categories; glycolytic intermediates (**A, D, G, J**), TCA cycle intermediates (**B, E, H, K**), and
765 amino acids (**C, F, I, L**). Metabolite abundances in *Aipl1*$^{-/-}$ (**A-C**) and *Pde6b*^{H620Q} RPE-choroid
766 tissue (**D-F**) was compared to metabolite abundances in RPE-choroid tissue from C57BL/6J
767 controls of a similar age. Metabolite abundances in RetΔGlut1 (**G-I**) and RodΔGlut1 RPE-
768 choroid tissue (**J-L**) was compared to metabolite abundances in RPE-choroid tissue from
769 uninjected or tamoxifen injected Glut1$^{fl/fl}$ controls of a similar age. Lactate levels were
770 consistently lower in the experimental groups of all tissues. n=5-6 per group.
771
772 **Figure 5. Mouse RPE-choroid uses photoreceptor-derived lactate *in vivo.* (A, B)** C57BL/6J
773 and *Aipl1* $^{-/-}$ mice were euthanized and their (**A**) retina or (**B**) RPE-choroid tissue were incubated
774 *ex vivo* in $^{13}C_6$-glucose. The amount of ^{13}C labeled DHAP, PEP, pyruvate, lactate, citrate,
775 succinate, and malate were quantified by mass spectrometry. *Aipl1*$^{-/-}$ decreases utilization of
776 glucose by the retina, but not the RPE-choroid. (**C, D**) Jugular vein catheters were installed in
777 C57BL/6J and *Aipl1*$^{-/-}$ mice. A bolus dose of 100 mg/kg $^{13}C_6$-glucose was infused through
778 jugular vein catheters, then mice were euthanized 1, 2, 3, or 5 minutes later. Tissue levels and
779 ^{13}C labeling of DHAP, PEP, pyruvate, lactate, citrate, succinate, and malate were determined
780 using mass spectrometry. ^{13}C labeling of labeling of metabolic intermediates was drastically
781 altered in both the (**C**) retina and (**D**) RPE-choroid of mice where the $^{13}C_6$-glucose had been
782 infused. (**E, F**) contain data from the same mice as **C** and **D**, but show the proportion of each
783 metabolite that is ^{13}C labeled. In all panels, “0 minute” samples were from retina or RPE-choroid
784 tissue that was not exposed to a ^{13}C fuel.

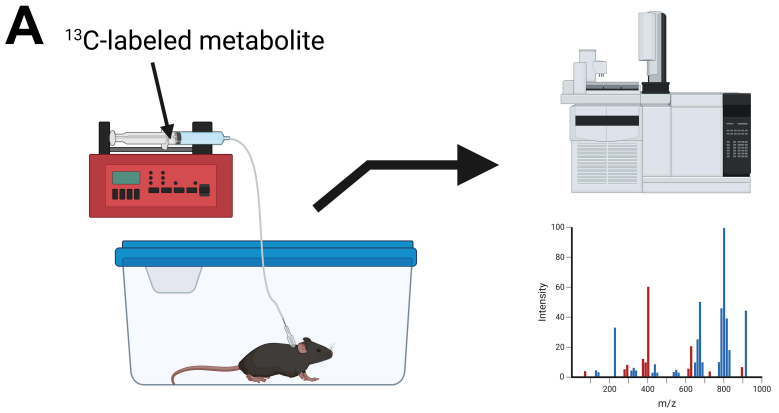
A
13C-labeled metabolite
Intensity
m/z

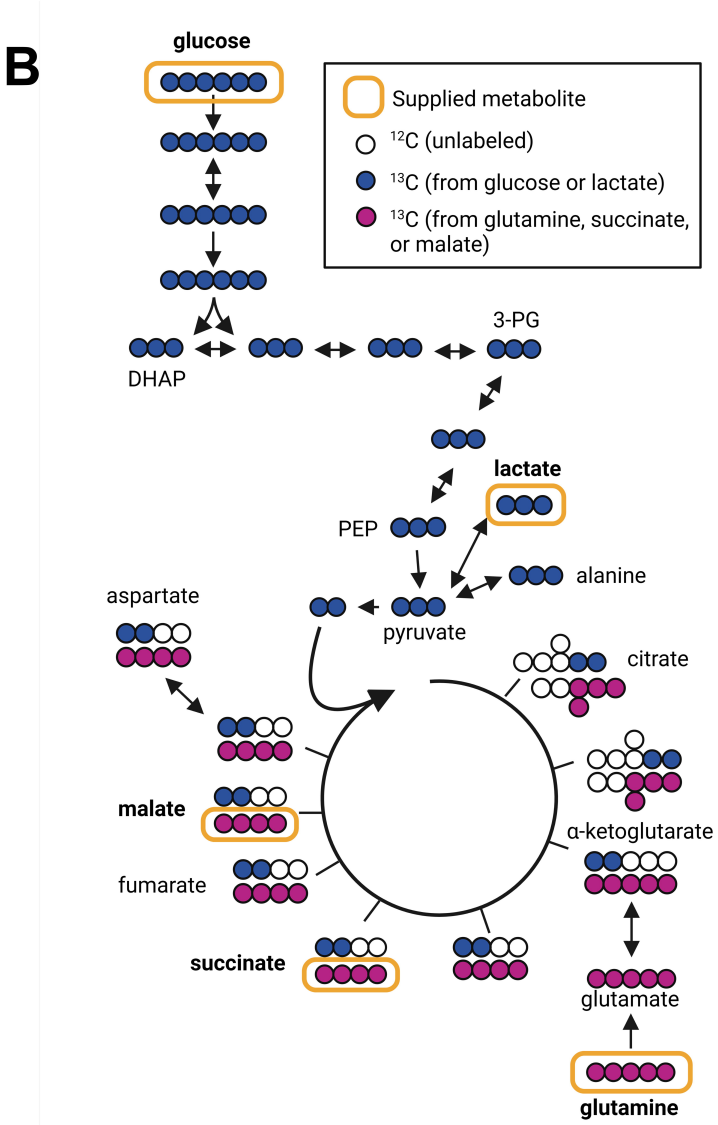
B
glucose
Supplied metabolite
12C (unlabeled)
13C (from glucose or lactate)
13C (from glutamine, succinate, or malate)
3-PG
DHAP
lactate
PEP
alanine
aspartate
pyruvate
citrate
malate
α-ketoglutarate
fumarate
succinate
glutamate
glutamine

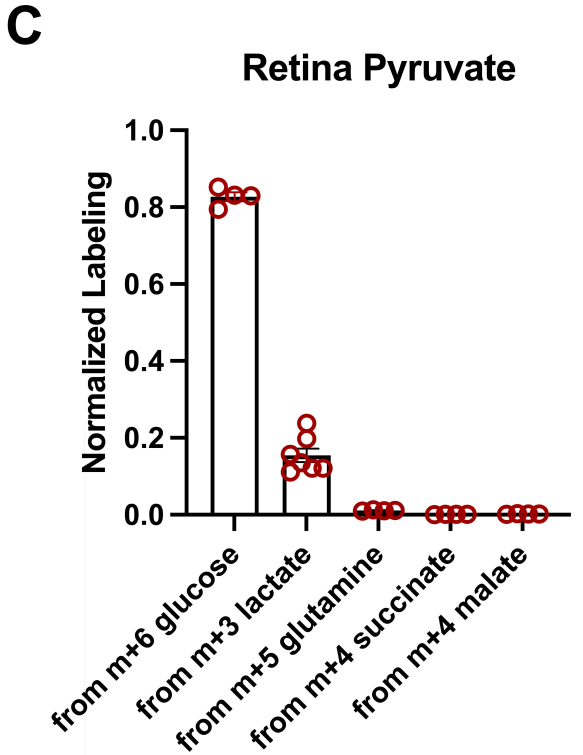
C
Retina Pyruvate
Normalized Labeling
1.0
0.8
0.6
0.4
0.2
0.0
from m+6 glucose
from m+3 lactate
from m+5 glutamine
from m+4 succinate
from m+4 malate

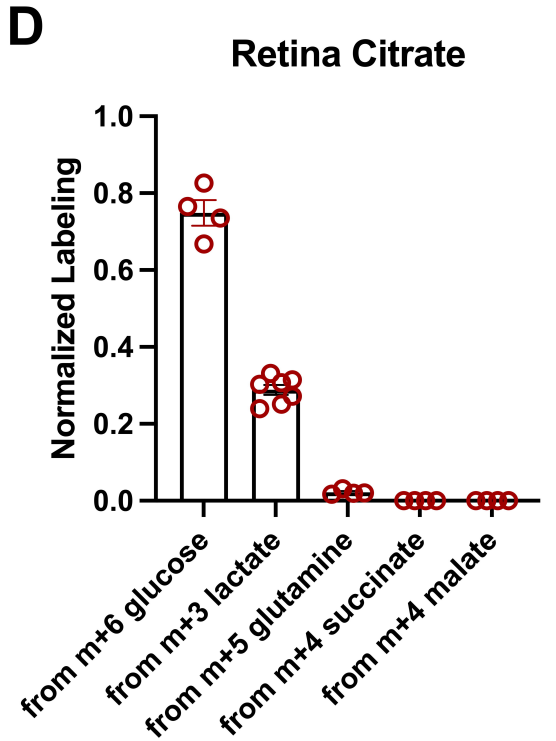
D
Retina Citrate
Normalized Labeling
1.0
0.8
0.6
0.4
0.2
0.0
from m+6 glucose
from m+3 lactate
from m+5 glutamine
from m+4 succinate
from m+4 malate

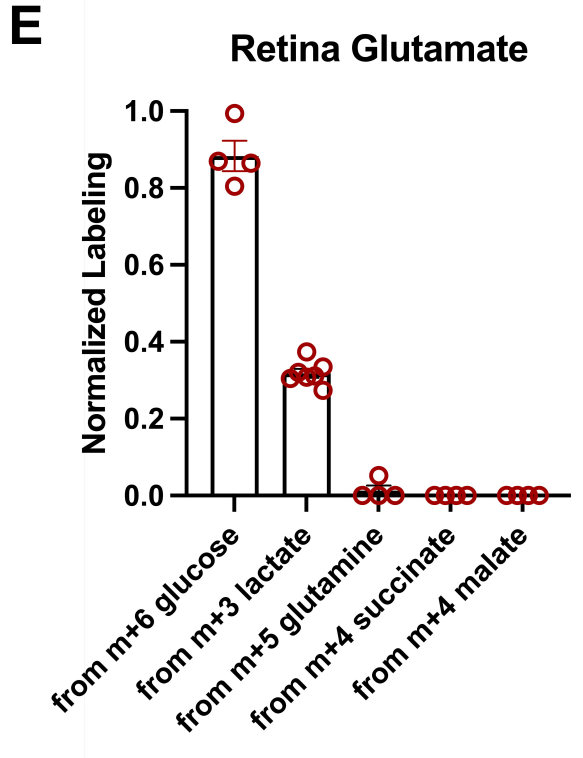
E
Retina Glutamate
Normalized Labeling
1.0
0.8
0.6
0.4
0.2
0.0
from m+6 glucose
from m+3 lactate
from m+5 glutamine
from m+4 succinate
from m+4 malate

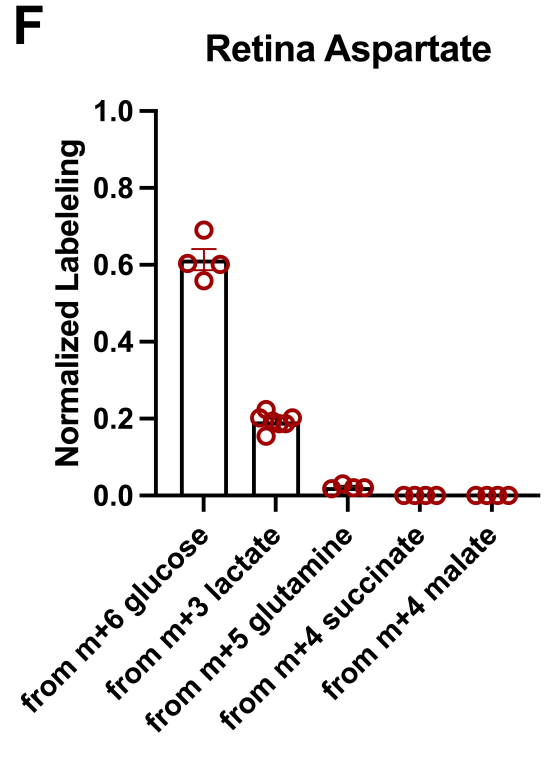
F
Retina Aspartate
Normalized Labeleling
1.0
0.8
0.6
0.4
0.2
0.0
from m+6 glucose
from m+3 lactate
from m+5 glutamine
from m+4 succinate
from m+4 malate

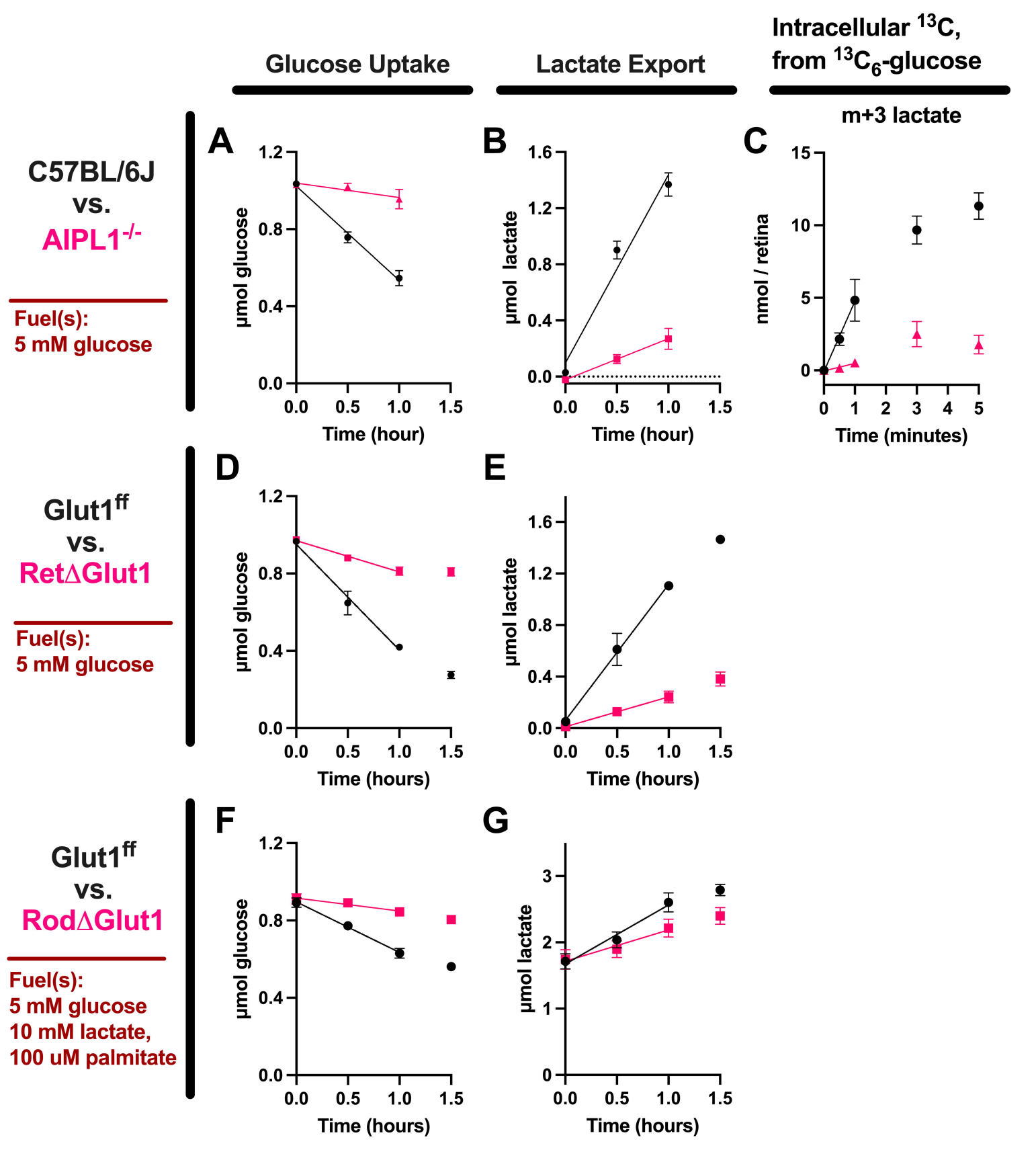
Glucose Uptake
Lactate Export
Intracellular 13C, from 13C6-glucose
m+3 lactate
C57BL/6J vs. AIPL1-/-
Fuel(s): 5 mM glucose
Glut1ff vs. RetΔGlut1
Fuel(s): 5 mM glucose
Glut1ff vs. RodΔGlut1
Fuel(s): 5 mM glucose 10 mM lactate, 100 uM palmitate
A
B
C
D
E
F
G
µmol glucose
µmol lactate
nmol / retina
Time (hour)
Time (minutes)
Time (hours)

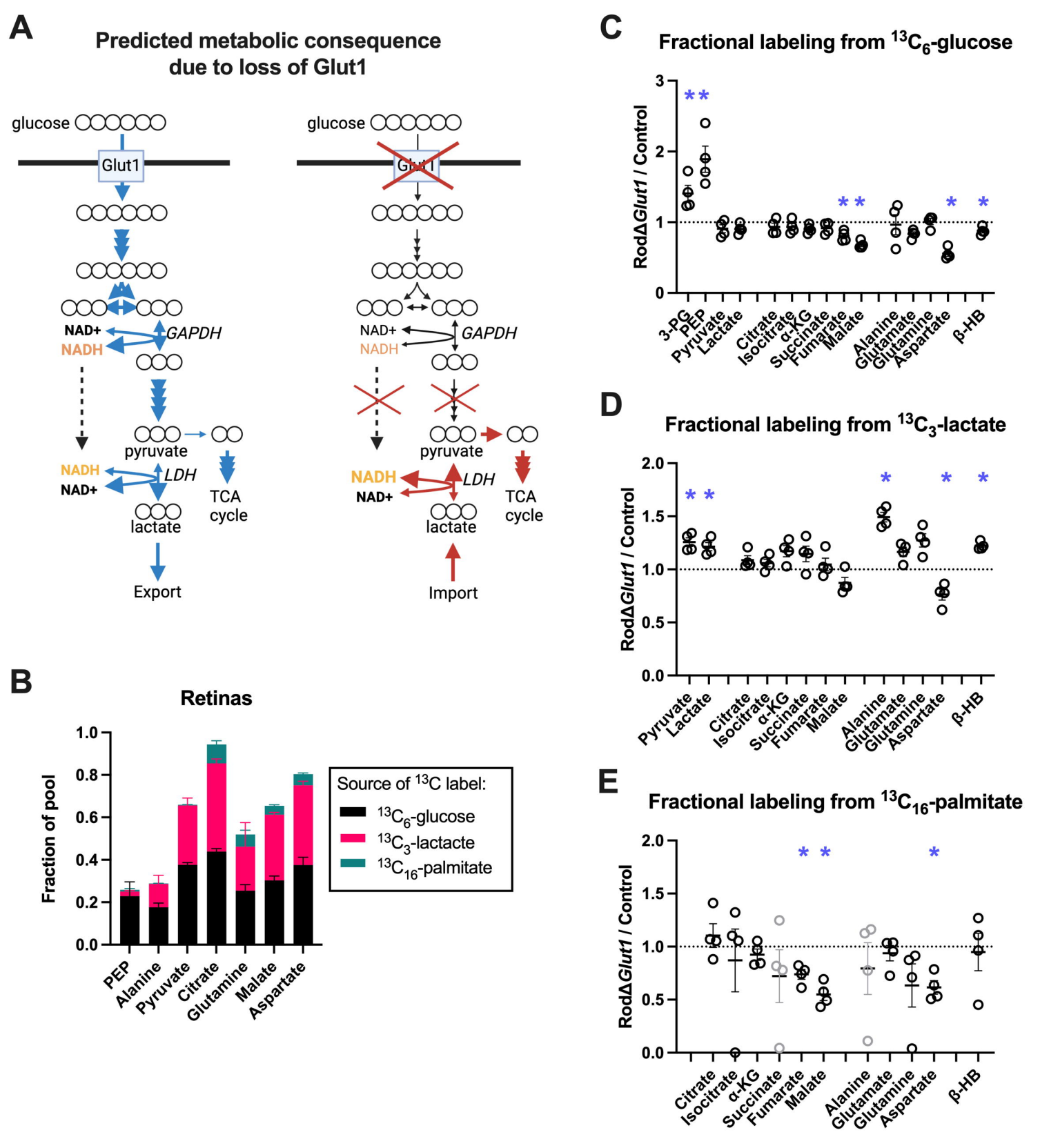
A
Predicted metabolic consequence due to loss of Glut1
glucose
Glut1
NAD+
NADH
GAPDH
pyruvate
NADH
NAD+
LDH
lactate
TCA cycle
Export
glucose
Glut1
NAD+
NADH
GAPDH
pyruvate
NADH
NAD+
LDH
lactate
TCA cycle
Import
B
Retinas
Fraction of pool
1.0
0.8
0.6
0.4
0.2
0.0
PEP
Alanine
Pyruvate
Citrate
Glutamine
Malate
Aspartate
Source of 13C label:
13C6-glucose
13C3-lactacte
13C16-palmitate
C
Fractional labeling from 13C6-glucose
RodΔGlut1 / Control
3
2
1
0
3-PG
PEP
Pyruvate
Lactate
Citrate
Isocitrate
α-KG
Succinate
Fumarate
Malate
Alanine
Glutamate
Glutamine
Aspartate
β-HB
D
Fractional labeling from 13C3-lactate
RodΔGlut1 / Control
2.0
1.5
1.0
0.5
0.0
Pyruvate
Lactate
Citrate
Isocitrate
α-KG
Succinate
Fumarate
Malate
Alanine
Glutamate
Glutamine
Aspartate
β-HB
E
Fractional labeling from 13C16-palmitate
RodΔGlut1 / Control
2.0
1.5
1.0
0.5
0.0
Citrate
Isocitrate
α-KG
Succinate
Fumarate
Malate
Alanine
Glutamate
Glutamine
Aspartate
β-HB

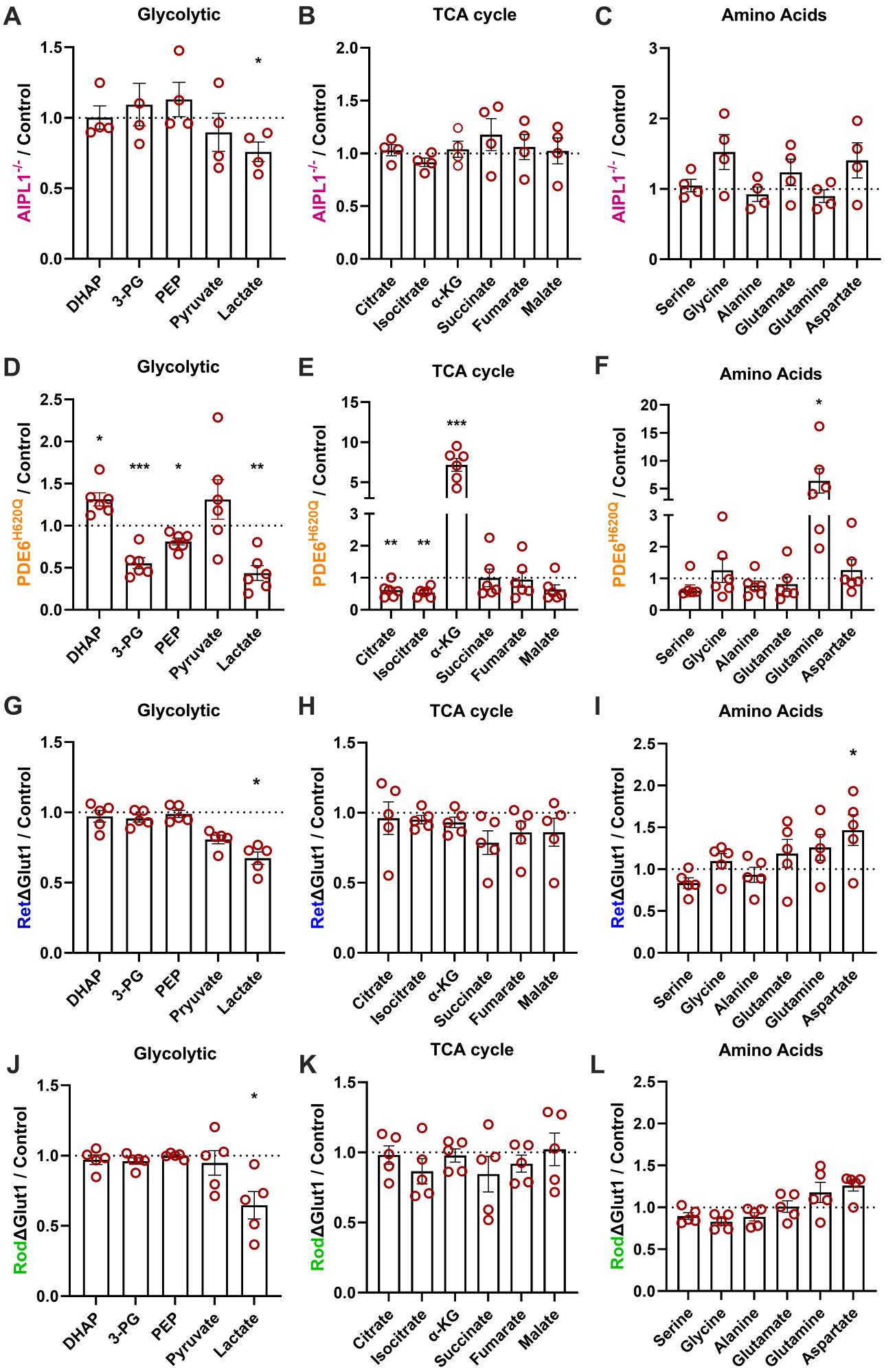
A
Glycolytic
AIPL1-/- / Control
DHAP
3-PG
PEP
Pyruvate
Lactate
B
TCA cycle
Citrate
Isocitrate
α-KG
Succinate
Fumarate
Malate
C
Amino Acids
Serine
Glycine
Alanine
Glutamate
Glutamine
Aspartate
D
PDE6H620Q / Control
E
F
G
RetΔGlut1 / Control
H
I
J
RodΔGlut1 / Control
K
L

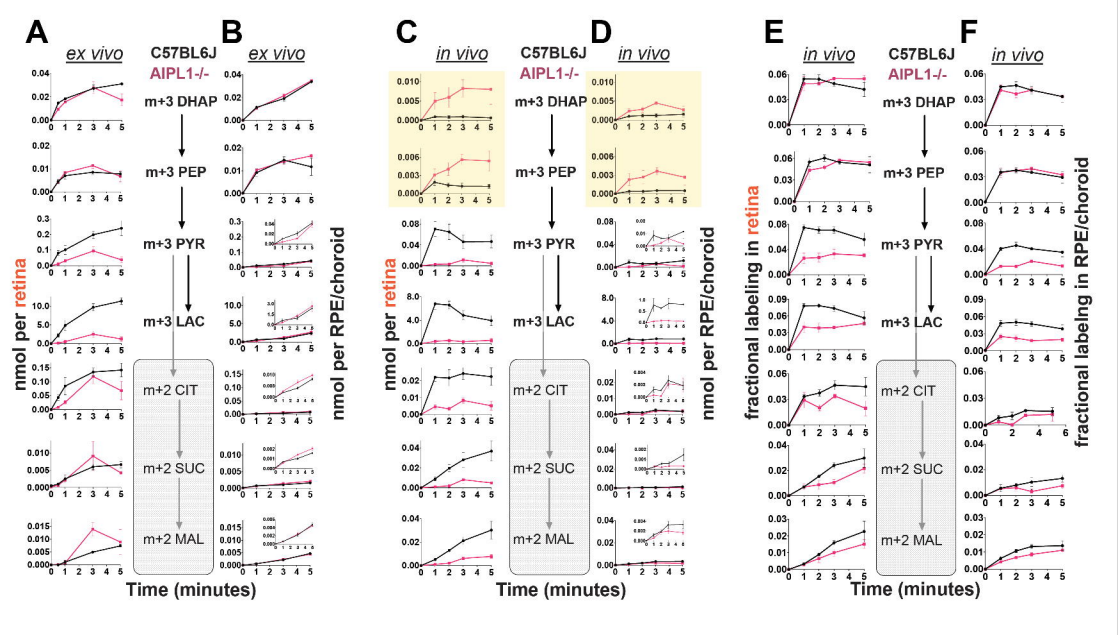
A
ex vivo
B
ex vivo
C57BL6J
AIPL1-/-
m+3 DHAP
m+3 PEP
m+3 PYR
m+3 LAC
m+2 CIT
m+2 SUC
m+2 MAL
nmol per retina
nmol per RPE/choroid
Time (minutes)
C
in vivo
D
in vivo
E
in vivo
F
in vivo
fractional labeling in retina
fractional labelng in RPE/choroid